INSTITUTE OF PHYSICS PUBLISHING JOURNAL OF PHYSICS: CONDENSED MATTER

J. Phys.: Condens. Matter **15** (2003) 347–365 PII: S0953-8984(03)53179-4

Bridging scales from molecular simulations to classical thermodynamics: density functional theory of capillary condensation in nanopores

Alexander V Neimark[1], **Peter I Ravikovitch and Aleksey Vishnyakov**

The Center for Modeling and Characterization of Nanoporous Materials, TRI/Princeton, 601 Prospect Avenue, Princeton, NJ 08542, USA

E-mail: aneimark@triprinceton.org

Received 9 September 2002, in final form 7 November 2002
Published 13 January 2003
Online at stacks.iop.org/JPhysCM/15/347

Abstract

With the example of the capillary condensation of Lennard-Jones fluid in nanopores ranging from 1 to 10 nm, we show that the non-local density functional theory (NLDFT) with properly chosen parameters of intermolecular interactions bridges the scale gap from molecular simulations to macroscopic thermodynamics. On the one hand, NLDFT correctly approximates the results of Monte Carlo simulations (shift of vapour–liquid equilibrium, spinodals, density profiles, adsorption isotherms) for pores wider than about 2 nm. On the other hand, NLDFT smoothly merges (above 7–10 nm) with the Derjaguin–Broekhoff–de Boer equations which represent augmented Laplace–Kelvin equations of capillary condensation and desorption.

1. Introduction

In studies of nanoscale systems, researchers confront two fundamental problems:

(i) how to reconcile molecular simulations dealing with an ensemble of interacting molecules confined by potential fields and classical thermodynamics operating with homogeneous phases separated by suitably defined interfaces; and
(ii) how to establish the limits of applicability of macroscopic equations of capillarity.

In this paper, we address these problems with the example of capillary condensation of the Lennard-Jones (LJ) fluid in nanopores with cylindrical LJ walls. We show that the non-local density functional theory (NLDFT) [1–3] with properly chosen parameters of intermolecular interactions [4, 5] bridges scales from molecular simulations to classical thermodynamics: NLDFT approximates the results of Monte Carlo (MC) simulations [6] for pores wider than

[1] Author to whom any correspondence should be addressed.

about 2 nm and, in turn, can be approximated by the macroscopic Derjaguin–Broekhoff–de Boer (DBdB) equations [7–9] for pores wider than 7–10 nm. Thus, the density functional theory, which operates with inhomogeneous phases characterized by coarse-grained densities, provides a reasonable compromise between the discrete approach of molecular simulations and the homogeneous representation of classical thermodynamics.

The paper is organized as follows. In section 2 we describe the phenomenon of capillary condensation in nanopores, present instructive experimental examples, and discuss general problems of experimental observations and theoretical analyses of metastable states and hysteretic phase transitions inherent to confined fluids. Special attention is paid to the role of constraints in the thermodynamics of hysteresis and to the specifics of phase equilibrium and criticality. In section 3, we discuss MC simulations of capillary condensation and focus on the gauge cell MC method [6, 10] designed for simulations of multiple metastable and labile states under appropriate constraints. In section 4, we present the canonical ensemble version of the NLDFT model of capillary condensation. In section 5, we compare the NLDFT results with the MC simulation data. Good agreement is found for sorption isotherms, density profiles, points of condensation transitions, and spinodals. A comparison of the NLDFT and MC results with the macroscopic Laplace–Kelvin and DBdB equations is made in section 6. In section 7, we demonstrate correlations with experimental data. Final conclusions are formulated in section 8.

2. Experimental specifics of capillary condensation. What do we want to understand?

Capillary condensation of vapours in pores of solids represents a prominent example of phase transitions in confined fluids. When a porous solid is exposed to the vapour of a wetting fluid, the latter condenses in pores at a vapour pressure lower than the saturation pressure at the given temperature. The pressure of condensation depends on the liquid–vapour interfacial tension, the adhesion interaction between the solid and the fluid, and the pore geometry, its size and shape. Capillary condensation is usually characterized by a step in the adsorption isotherm. In materials with a uniform pore size distribution, the capillary condensation step is notably sharp, as exemplified by the adsorption of vapours on ordered mesoporous molecular sieves templated on regular surfactant or block-copolymer mesophases. In figure 1 we present a typical example of argon adsorption at its boiling temperature 87 K on a series of MCM-41-type samples possessing regular arrays of cylindrical channels of different diameters [11, 12]. In pores wider than about 5 nm, capillary condensation is associated with an apparent hysteresis: as the vapour pressure decreases, the desorption occurs at a pressure lower that the pressure of condensation. Everett [13] has named this irreversible behaviour a *permanent hysteresis*, emphasizing that the hysteresis loop is reproducible in adsorption experiments performed with a sufficient equilibration time and does not depend on the number of repeatable sorption–desorption cycles. Here, we are dealing with long-living metastable states separated from the stable states by insurmountable, at given experimental conditions, energy barriers. The permanent hysteresis takes place when the observation time is much larger than the time of relaxation to a given metastable state and is much smaller than the characteristic time of nucleation of the stable phase. This situation is typical for confined fluids which are characterized by multiple equilibrium states, metastability, and hysteretic phase transformations [14]. Indeed, the constraints imposed by confinement reduce the level of thermal density fluctuations, so the nucleation is severely suppressed and the system remains in a metastable state over the experimentally 'infinite' time. As the pore size decreases, the experimental hysteresis loop gradually narrows, and finally disappears for pores smaller than about 4 nm.

According to a traditional viewpoint [15, 16], the disappearance of hysteresis indicates the critical conditions of capillary condensation as the first-order phase transition and thus

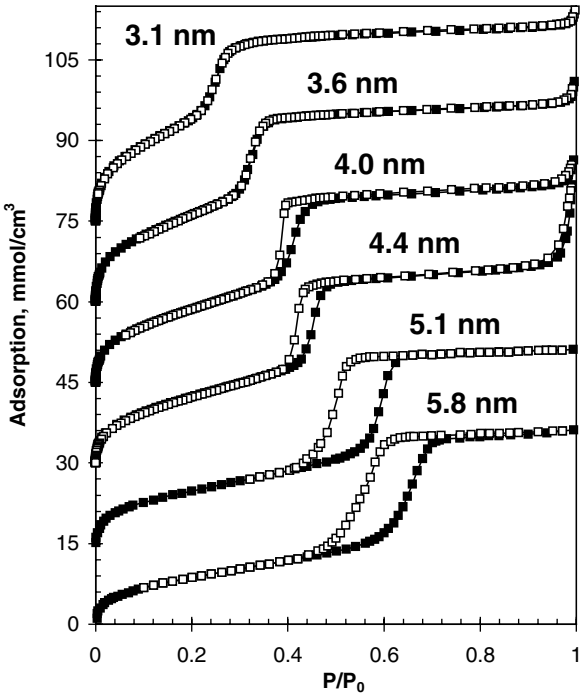

Figure 1. Experimental adsorption and desorption isotherms of Ar at 87 K on a series of mesoporous molecular sieves with cylindrical pores of characteristic diameter 3.1, 3.6, 4.0, and 4.4 nm [11], and 5.1 and 5.8 nm [73].

determines the shift of the critical temperature for a pore from the bulk value T_c to a lower temperature T_{cc}, which is called the pore critical temperature. The smaller the pore, the lower the pore critical temperature T_{cc}. Consequently, during adsorption isothermal measurements at a given subcritical temperature T, liquid–vapour phase separation is possible only in pores wider than the critical pore size D_{cc}. The critical pore size D_{cc} decreases as the temperature decreases. Thus, under this assumption the critical pore size D_{cc} for argon adsorption at 87 K from experimental data given in figure 1 is estimated as $\sim$4 nm.

However, reliable experimental verifications of the capillary condensation theory for nanopores were not available prior to the early 1990s due to the lack of materials with a well characterized pore structure. Theoretical hypotheses and conclusions were supported by experiments with silica gels, porous glasses, and other systems with a disordered pore structure that prevented an unambiguous theoretical treatment. The discovery in 1992 [17, 18] of the ordered mesoporous molecular sieves of MCM-41 type has opened a unique opportunity to test theoretical predictions. MCM-41-type materials possess a uniform system of cylindrical channels of controlled diameter, which can be evaluated independently. These materials are considered now as the most suitable references for adsorption measurements.

The first experiments of Ravikovitch *et al* [4] with reference MCM-41 samples have shown that the disappearance of hysteresis cannot be explained as the achievement of the critical conditions of capillary condensation as the first-order phase transition. It was demonstrated that at elevated temperatures and/or in sufficiently narrow pores the capillary condensation in open-ended cylindrical pores occurs reversibly without a hysteresis. This concept was elaborated by Morishige and Shikimi [19] who, in addition to the pore critical temperature T_{cc}

and the critical pore size D_{cc}, introduced the hysteresis critical temperature T_{ch}, which is lower than T_{cc}, and the hysteresis critical pore size D_{ch}, which is larger than D_{cc}. The authors [19] proposed a special protocol for experimental determination of the critical temperature of capillary condensation as the first-order phase transition, T_{cc}, and showed that it exceeds the hysteresis critical temperature, T_{ch}. For example, for Ar sorption on a sample of MCM-41 material with channels of 2.2 nm, the hysteresis critical temperature and the pore critical temperature were estimated as $T_{ch} \approx 62$ K and $T_{cc} \approx 98$ K [19]; see also the latest paper of Morishige and Masataka [20]. Thus, it is implied that for a given fluid–solid pair, three regimes of sorption are distinguished experimentally, depending on the temperature T and the pore diameter D:

(i) at $T > T_{cc}$, $D < D_{cc}$, adsorption occurs at supercritical conditions without a stepwise transition from a low-density vapour-like phase to a high-density liquid-like state;
(ii) at $T_{ch} < T < T_{cc}$, $D_{cc} < D < D_{ch}$, a stepwise capillary condensation transition takes place reversibly without hysteresis;
(iii) at $T_c < T < T_{ch}$, $D_{ch} < D$, capillary condensation exhibits hysteresis.

These three regimes of sorption were qualitatively confirmed in MC simulations (see section 5 below).

To avoid possible misinterpretations of the notions of the pore critical temperature T_{cc} and the hysteresis critical temperature T_{ch}, let us recall that we study vapour–liquid transformation in essentially finite-volume systems and the experiments and simulations that we analyse are performed over a finite time. There is neither true phase equilibrium in terms of the thermodynamic limit, nor a true critical point with the infinite correlation length. By phase equilibrium in a finite system we mean the conditions at which there exist two equilibrium states of different density (vapour-like and liquid-like) with equal grand thermodynamic potentials. Consequently, by the pore critical temperature T_{cc} we mean the temperature at which these two states merge and above which there exists just one 'supercritical' equilibrium state. In this paper, we consider phase transitions in cylindrical pores that may seem to be in apparent contradiction with the Landau theorem [21], which forbids true phase transitions in one-dimensional systems with short-range interactions. Here, we deal with cylindrical pores of finite length, and as shown in [6] and recently in [22], even when the ratio L/D of the pore length to the pore diameter is large (for pores in MCM-41 materials, $L/D \sim 10^3$), this geometry cannot be treated as quasi-one-dimensional since at $T < T_{cc}$ the equilibrium concentration of interfaces, which is reciprocal to the exponent of the interfacial free energy, is extremely low—many orders of magnitude less than practically relevant values $(L/D)^{-1}$. Near T_{cc}, this strong inequality is no longer valid, and equilibrium configurations in long pores consist of sequences of liquid bridges and bubbles, as shown in numerous simulations of phase separation in cylindrical geometry [23–28]. However, at $T < T_{cc}$ this domain structure was not observed in MC simulations of quite long cylindrical capillaries of $L/D = 36$ [22].

To study metastable states and hysteretic phase transformations one has to control the level of allowed fluctuations by imposing certain constraints on the system under consideration. In macroscopic thermodynamic theories and mean-field approximations of statistical mechanics such as the density functional theories [15], which operate with a finite number of averaged quantities and functions, the constraints are enforced explicitly. In particular, if we restrict the probe functions in the canonical ensemble density functional theory to spatially uniform distributions possessing a symmetry compliant with the confinement geometry, the solution of the Euler equation at the fixed averaged density gives a continuous trajectory of states in the form of the adsorption isotherm which, in the coordinates density versus chemical potential or pressure, has a sigmoid shape similar to that of the van der Waals equation of state.

3. Monte Carlo simulations of capillary condensation. The gauge cell method

In molecular simulations, the metastable states can be stabilized by restricting, in one way or another, the sampling in order to avoid non-uniform configurations which may give rise to the development of critical nuclei. Following the pioneering papers of Penrose and Lebowitz [29, 30], several attempts were made to formulate the statistical mechanics of metastable phases using restricted ensembles [31–33]. MC simulations in restricted ensembles were performed for modelling metastable states in bulk fluids [31]. We have recently developed a new method for MC simulations of confined fluids in the region of metastability [6, 10]. In this method, called the gauge cell method, the density fluctuations are suppressed by considering the finite-volume system under study in equilibrium with a reference gauge cell which has a limited capacity. The level of density fluctuations in the system is controlled by the capacity of the gauge cell. In the limiting cases of infinitely large and infinitesimally small capacities, the gauge cell method corresponds respectively to the conventional schemes of grand canonical ensemble and canonical ensemble simulations.

In [6, 10], the gauge cell method was applied to study capillary condensation of LJ fluids in cylindrical nanopores with wetting walls. The simulations were performed with the parameters of fluid–fluid and fluid–solid interactions chosen to mimic adsorption of argon and nitrogen in cylindrical pores of siliceous mesoporous molecular sieves of MCM-41 type. For a series of pores of different diameters, we have determined the adsorption isotherms, the density of adsorbed fluid as a function of the chemical potential or of the vapour pressure. The constraints imposed on the system ensured that the states constructed in simulations corresponded to laterally uniform configurations. For relatively wide pores, the adsorption isotherm forms a continuous sigmoid-shaped trajectory similarly to the van der Waals loop typical for a first-order transition.

The sorption isotherm constructed, a typical example of which is presented in figure 2, is comprised of three parts:

(a) the adsorption branch ABS_V corresponds to uniform adsorption films on pore walls; these low-density states are called vapour-like since the density in the pore centre is close to the bulk vapour density;
(b) the desorption branch HFS_L corresponds to the condensed fluid; these states are called liquid-like since their density is close to the bulk liquid density;
(c) the backward trajectory S_VDS_L consists of states which would be unstable if the constraints imposed were removed.

The chemical potential μ_e of the equilibrium transition between the vapour-like B and liquid-like E states is determined by the thermodynamic integration in accord with the Maxwell rule: area BS_VB equals area FS_LD. The chemical potential μ_e of the equilibrium transition separates stable and metastable states. At $\mu < \mu_e$, the adsorption branch AB corresponds to the stable adsorption films while the desorption branch FS_L corresponds to the metastable stretched liquid. The turnover point S_L is the liquid-like spinodal, which represents the limit of mechanical stability of a stretched condensed liquid. At $\mu > \mu_e$, the desorption branch HF corresponds to the stable condensed liquid while the adsorption branch BS_V corresponds to the metastable adsorption films. The turnover point S_V is the vapour-like spinodal, which represents the limit of mechanical stability of metastable adsorption films. In an unconstrained system, the points of spontaneous condensation and desorption are determined by the nucleation barriers at given experimental conditions.

For comparison, in the same figure we present the results of GCMC simulations: point C corresponds to the spontaneous condensation and point E corresponds to the spontaneous

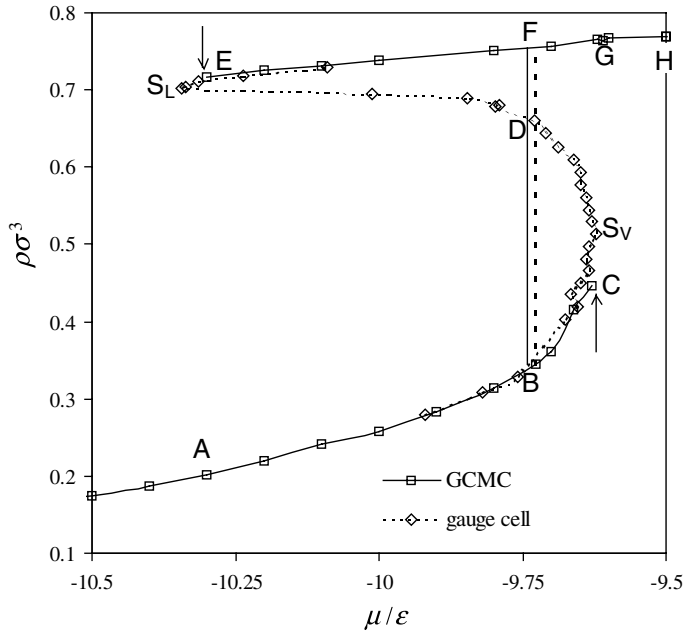

Figure 2. Nitrogen adsorption isotherms for a 6.9 nm cylindrical pore at 77.4 K ($kT/\varepsilon = 0.762$) calculated using the GCMC and gauge cell methods [10]. Vertical lines show the vapour–liquid coexistence in pores calculated with the gauge cell method (bold dashed line) and the thermodynamic integration technique of Peterson and Gubbins [74] (thin solid curve). Points: B—the vapour-like state at vapour–liquid coexistence; C—the limit of stability of the vapour-like phase in the GCMC method (the fluid undergoes a spontaneous transition to point G); S_V—the vapour-like spinodal; D—an unstable state, S_L—the liquid-like spinodal; E—the limit of stability of the liquid-like phase in the GCMC method (the fluid undergoes a spontaneous transition to point A); F—the liquid-like state at vapour–liquid coexistence; H—the stable liquid-like state at vapour–liquid coexistence for bulk fluid.

evaporation. While the metastable states in the vicinities of spinodals, CS_V and ES_L, were not accessible in GCMC simulations, the results of the gauge cell and GCMC simulations are in remarkable agreement. The dotted line indicates the point of equilibrium transition determined from the hysteretic GCMC isotherm determined by the Peterson–Gubbins method of thermodynamic integration [14], circumventing the spontaneous transitions through the supercritical region.

In the simulations considered below, the number of molecules in the pore cell varied from 2000 in the largest pore to 300 in the smallest. The number of molecules in the gauge cell was 30–60 in all simulations. In the simulation conditions, the fluid in the gauge cell behaved as an ideal gas. Thus, since the fluctuations in the pore cell and in the gauge cell are coupled, the variations of the number of molecules in the pore cell did not exceed about 2%. In these conditions, the average values of thermodynamic quantities obtained in the gauge cell simulation were indistinguishable from those in the CEMC method, and also from the results of the GCMC method in the case of hysteresis at $T < T_{ch}$, as illustrated in figure 2. The discrepancies between the results for different ensembles identify the regime of reversible condensation at $T_{ch} < T < T_{cc}$.

As shown in [6], MC simulations quantitatively describe the experimental sorption isotherms for reference nanoporous materials such as those shown in figure 1. However,

detailed MC simulations for larger pores require prohibitively long computation times. At the same time, one expects that for sufficiently wide pores the capillary condensation should follow the macroscopic laws of capillarity, such as Laplace and Kelvin equations, which become progressively more inaccurate as the pore diameter decreases to the nanometre range [4, 34–38]. In order to reconcile the molecular simulations and the macroscopic theory of capillarity, we apply the NLDFT in the canonical ensemble.

4. Canonical ensemble density functional theory

The DFT implies that the Helmholtz free energy, F, of a confined fluid is represented as a functional of the spatially varying fluid density $\rho(\boldsymbol{r})$. Introduction of the spatially varying density of molecules seems to be a reasonable compromise between the abrupt density changes in classical thermodynamics and the discrete enumeration of fluctuations in molecular simulations. Several versions of DFT for inhomogeneous fluids were formulated [3, 39–42]. They differ in how they account for intermolecular correlations. The basic formulations of the DFT of inhomogeneous fluids can be found in [1, 43, 44]. However, almost any version of DFT treats attractive interactions in a mean-field approximation, whose validity for a quantitative description of a given phenomenon can be justified only by comparing with direct molecular simulations.

Different DFT models were proposed for studies of vapour–liquid equilibrium, wetting and layering transitions, structure of simple fluids, and single-component and binary mixture adsorption (see [1, 14, 45] for reviews). In this paper we employ the NLDFT with the functional developed by Tarazona [2, 3] and known as the smoothed density approximation (SDA). This version of NLDFT was used efficiently for studying adsorption in model pores [46, 47]. In particular, in our earlier papers we have shown that this model, implemented for a LJ fluid confined by solid layers of immobile LJ centres with suitably chosen parameters of fluid–fluid and fluid–solid intermolecular potentials, gives good agreement with experimental data on capillary condensation of argon and nitrogen in cylindrical [4, 35, 36, 48] and spherical [38] pores of mesoporous molecular sieves, and adsorption of nitrogen, methane, krypton, and other gases in slit-shaped pores of carbons [49–51]. The NLDFT model constitutes a basis of the new methods for pore size distribution analysis of nanoporous materials [34, 36, 37, 46, 47, 51].

Conventional versions of the DFT imply minimization of the grand thermodynamic potential with respect to the fluid density within fixed solid boundaries at given temperature T and chemical potential μ [1]. They correspond to the grand canonical (μ–V–T) ensemble. In order to generate continuous isotherms, which, similarly to the gauge cell MC simulations (figure 2), trace stable, metastable, and labile states in a van der Waals manner, we apply the DFT in the canonical (N–V–T) ensemble. While the canonical ensemble DFT was efficiently used for modelling nucleation in the bulk fluids [52], its application to capillary condensation was suggested first in [53]. Several lattice and off-lattice versions of DFT in the canonical ensemble have been reported and discussed recently [54–62].

We consider a closed system consisting of N molecules of fluid confined in a volume V surrounded by solid walls. The system is embedded in a bath of constant temperature T. The fluid is modelled as a soft-sphere fluid with a given pairwise attractive potential, $\Phi_{\mathrm{ff}}(\boldsymbol{r}_1, \boldsymbol{r}_2)$. The fluid–solid interactions are modelled by a given spatially varying external potential, $\Phi_{\mathrm{sf}}(\boldsymbol{r})$. Equilibrium states of the closed system are defined by minimization of the Helmholtz free energy functional at constant N, V, and T. The DFT implies that the intrinsic Helmholtz free energy, F_{int}, depends entirely upon given fluid–fluid interaction potential(s), $\Phi_{\mathrm{ff}}(\boldsymbol{r}_1, \boldsymbol{r}_2)$, and is represented as a functional of the spatially varying fluid density $\rho(\boldsymbol{r})$. The external solid–fluid interaction potential, $\Phi_{\mathrm{sf}}(\boldsymbol{r})$, does not affect the expression for intrinsic Helmholtz free energy

functional, $F_{\rm int}[\rho(\boldsymbol{r}),\,\Phi_{\rm ff}]$, and makes an additive contribution, $F_{\rm ext}[\rho(\boldsymbol{r}),\,\Phi_{\rm sf}]$, to the total Helmholtz free energy, F:

$$F[\rho(\boldsymbol{r})] = F_{\rm int}[\rho(\boldsymbol{r}),\,\Phi_{\rm ff}] + F_{\rm ext}[\rho(\boldsymbol{r}),\,\Phi_{\rm sf}]. \tag{1}$$

Equilibrium states in the canonical ensemble are obtained by minimization of the Helmholtz free energy functional (1) with respect to the fluid density $\rho(\boldsymbol{r})$, provided that the total number of molecules is a given constant N:

$$\int_V \rho(\boldsymbol{r})\,\mathrm{d}\boldsymbol{r} = N. \tag{2}$$

To find a solution of this conditional extremum problem, one has to solve the Euler equation for the functional

$$\Omega[\rho(\boldsymbol{r})] = F[\rho(\boldsymbol{r})] - \mu\int_V \rho(\boldsymbol{r})\,\mathrm{d}\boldsymbol{r}. \tag{3}$$

Here, an additional unknown parameter, μ, is introduced. The Euler equation for the functional (5) reads

$$\mu = \frac{\delta F}{\delta\rho}. \tag{4}$$

Here, $\delta/\delta\rho$ denotes the functional derivative. The right-hand side of the equation (4) depends on the representation employed for the intrinsic Helmholtz free energy functional, $F_{\rm int}[\rho(\boldsymbol{r})]$. Equations (4) and (2) represent a closed system for determination of two unknowns, a function $\rho(\boldsymbol{r})$ and a constant μ. The solution gives the equilibrium density profile $\rho(\boldsymbol{r}, N, V, T)$ and the value of $\mu(N, V, T)$, which turns out to be equal to the chemical potential of the corresponding N, V, T state. Hence, the functional $\Omega[\rho(\boldsymbol{r}, N, V, T), \mu(N, V, T)]$ is equal to the grand potential. Note that the system does not imply a unique solution at given N [63]. The chemical potential obtained, μ, is not necessarily a single-valued function of N. In the region of a phase transition there may exist multiple equilibrium states and an additional analysis is required to select between stable, metastable, and labile states. Constraints imposed on trial functions reduce the number of admissible states. For example, while considering capillary condensation in cylindrical channels we restrict ourselves to laterally uniform symmetric configurations assuming that the fluid density is one-dimensional and depends on the distance to the pore centre. Because of this, non-uniform equilibrium configurations such as menisci, liquid bridges, and bubbles are ruled out of consideration. Typically, the functions $N(\mu)$ determined within constraints of uniformity consistent with the channel symmetry are non-monotonic and exhibit S-shaped swings in the regions of first-order phase transitions.

It should be noted that the CEDFT procedure described above is not rigorously consistent with the statistical mechanics foundations behind the density functional theory [64, 65]. We apply in CEDFT the same free energy functional as in GCDFT, restricting the density to a given constant. This procedure gives exactly the same equilibrium states as GCDFT and provides an analytical extension over the region of labile states, thus spanning the gap between equilibrium adsorption and desorption isotherms. Indeed, in finite-volume systems the radial distribution functions in the canonical and grand canonical ensembles differ [66], as well as the mean-density profiles in the CE and GC for the states of equal density. To address this problem, Gonzalez *et al* [58, 60, 62] suggested a rationale for recalculating the GC density profiles as their CE counterparts. Recently, White *et al* [61] augmented the free energy functional of GCDFT to provide consistent results in CEDFT. Hernando and Blum [58] and Hernando [62] attempted to construct a rigorous approach to CEDFT based on a hierarchy of correlation and distribution functions. However, appreciable deviations between CEDFT and GCDFT were

found in extreme confinements such as a spherical pore, which can accommodate just a few guest molecules [54, 60, 61]. The smallest confinement considered here is significantly larger, so the approach that we use is justified. The extension of the mean-field density functional over the region of labile states naturally produces continuous loops of van der Waals type.

5. Capillary condensation of Ar in cylindrical pores. Comparison of DFT and MC results

As an example of CEDFT calculations, we present in figure 3 the capillary condensation isotherms of Ar in a series of cylindrical pores mimicking pore channels in MCM-41 mesoporous molecular sieves. The isotherms are presented in the coordinates adsorption N versus relative pressure P/P_0. Calculations were performed at 87 K for internal diameters ranging from 1.43 to 100 nm. We used Tarazona's SDA representation of the Helmholtz free energy [2, 3] with parameters for fluid–fluid and solid–fluid interaction potentials, which were validated in our previous papers [11]. A detailed description of the model can be found in [5]. The density profiles were determined by solving the Euler equation (4) with the condition (2) by means of the Broiden method [67]. It is important to note that the fluid–fluid interaction parameters were chosen to give the best fit to the bulk equilibrium experimental data including the vapour and liquid densities and also the liquid surface tension at the given temperature. They differ somewhat from the fluid–fluid parameters used in MC simulations which in turn provided the best fit to the bulk equilibrium data. The fluid–solid interaction parameters were chosen to reproduce a reference Ar isotherm for non-porous silica. For a justification of the parameters employed, see [5].

The isotherms presented in figure 3 correspond to the pore sizes for which we performed MC simulations earlier [6]. The pore dimensions in figure 3 represent internal diameters of channels. The results of the GCMC and gauge cell MC simulations are given for comparison. For pores wider than 3 nm (figure 3, right panel), the NLDFT and MC isotherms agree remarkably well. NLDFT isotherms reproduce well the density of condensed fluid on the desorption branch HS_L, the thickness of an adsorbed layer on the adsorption branch AS_V, and also the density of the labile states on the unstable backward branch S_LS_V. Figure 4 demonstrates a typical example of almost identical density profiles determined by NLDFT and constructed in MC simulations. The positions of equilibrium transitions and vapour-like as well as liquid-like spinodals coincide within an experimentally negligible error; see figure 5. In figure 6 we show plots of the grand thermodynamic potential along the NLDFT and MC isotherms for 5.54 nm pores. The NLDFT grand thermodynamic potential was determined directly from equation (3), while the MC grand thermodynamic potential was calculated by thermodynamic integration along the continuous MC isotherm. The intersection point E in figure 6, which corresponds to the merging points B on the adsorption branch and F on the desorption branch (see figures 2 and 3), indicates the equality of the grand thermodynamic potentials of vapour-like and liquid-like states at equilibrium. The equilibrium chemical potential, μ_e, at point E can be defined from Maxwell's rule of equal areas by integrating along the S-shaped isotherm in coordinates N versus μ between the coexisting states:

$$\int_{N_B(\mu_e)}^{N_F(\mu_e)} \mu \, \mathrm{d}N = \mu_e(N_F - N_B). \tag{5}$$

The results of GCMC simulations are given in the same plots (figures 2, 3). Since in GCMC simulations, fluid within the pore is considered as an open system without imposing special constraints on density fluctuations, adsorption and desorption trajectories of GCMC states form a hysteresis loop with abrupt capillary condensation and desorption transitions. In

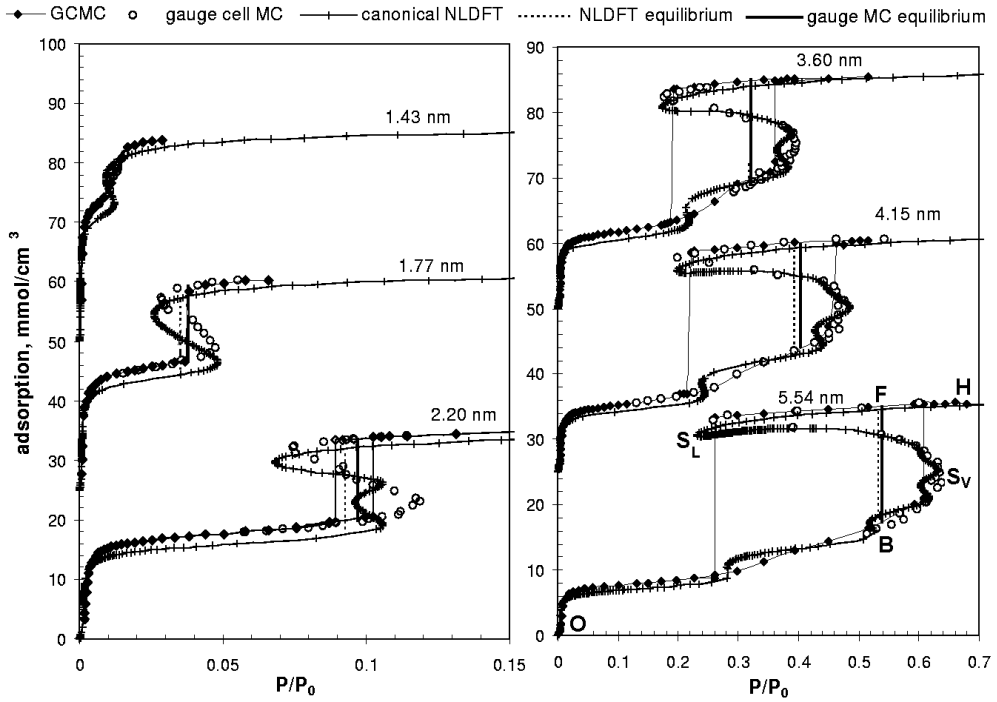

Figure 3. Argon adsorption isotherms for cylindrical pores at 87.3 K obtained using MC simulations and NLDFT. Vertical solid lines indicate spontaneous condensation and desorption in GCMC simulations. The thick solid vertical line shows the vapour–liquid coexistence in the pores obtained using the gauge cell method; the vertical broken line shows the vapour–liquid equilibrium obtained from NLDFT.

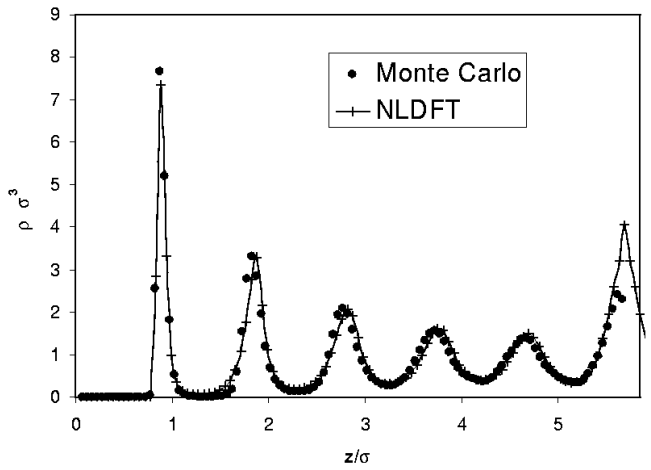

Figure 4. Local density profiles of Ar in an 11 σ (3.4 nm internal diameter) cylindrical pore at 87.3 K and $P = P_0$.

wider pores, these spontaneous transitions occur near the spinodal points. As the pore size decreases, the hysteresis loop of GCMC states narrows and disappears for a ∼2 nm pore, which

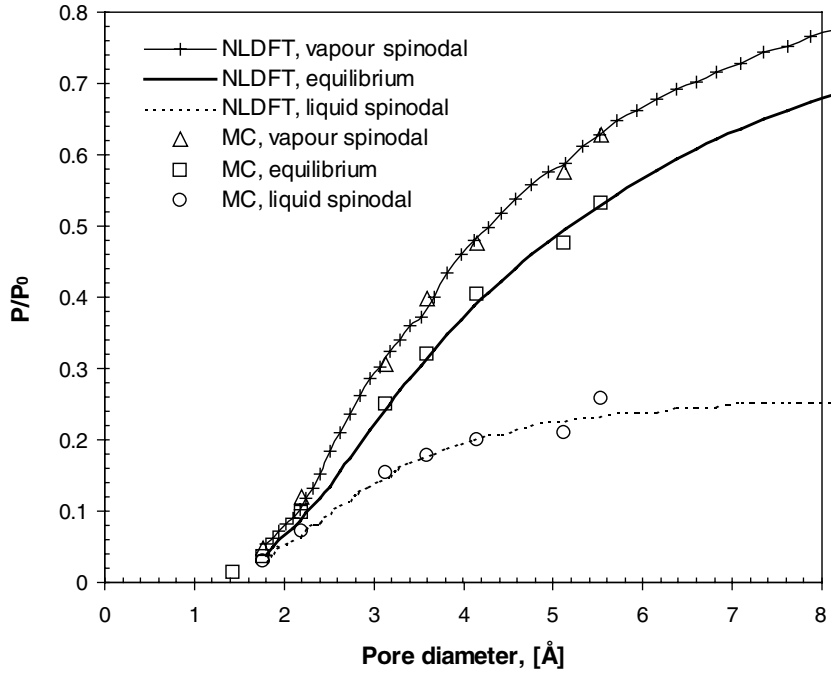

Figure 5. The conditions of spinodal condensation, desorption, and vapour–liquid coexistence of argon in a series of cylindrical pores at 87.3 K obtained using NLDFT and MC simulations.

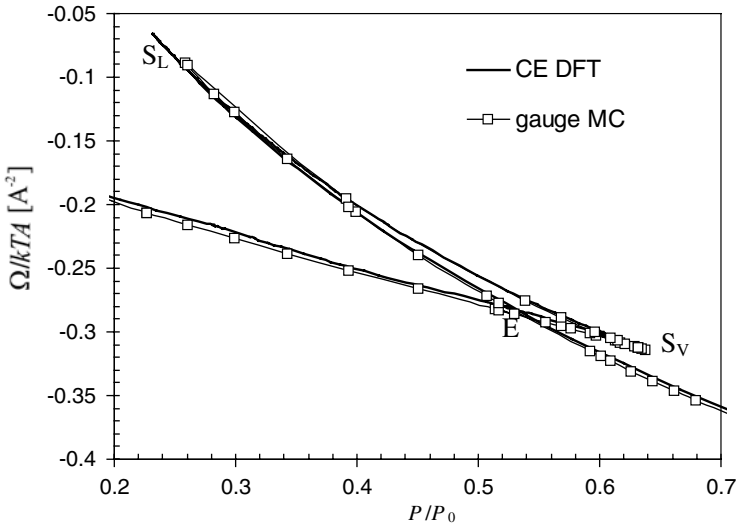

Figure 6. Isotherms of the grand potential of argon in a 5.54 nm cylindrical pore at 87.3 K obtained from thermodynamic integration along the MC and NLDFT adsorption isotherms. The intersection of the adsorption and desorption branches (point E) determines the vapour–liquid equilibrium.

is still subcritical, since both the gauge cell MC simulation and the CEDFT method distinguish low-density (adsorption, or vapour-like) and high-density (desorption, or liquid-like) states.

For supercritical pores, narrower than ∼1.5 nm, the MC isotherm is reversible, regardless to the simulation method.

Thus, in GCMC simulations, which mimic sorption from a vapour reservoir, we observe the same qualitative picture of three regimes of sorption as that observed experimentally: hysteretic condensation–evaporation in pores of $D > D_{ch} \approx 2$ nm, supercritical sorption in pores of $D < D_{cc} \approx 1.5$ nm, and reversible condensation in intermediate pores. In the latter case, the GCMC isotherm is rounded and, as shown in [6], the system during the simulation run jumps up and down, overcoming nucleation barriers from the low-density state to the high-density state. Note that while the value of the critical pore size D_{cc} is an objective quantity, the critical size of the hysteresis D_{ch} depends on the length of the simulation run (or the time of observation): the longer the run, the larger the probability of nucleation—and, consequently, D_{ch} increases. In the mathematical limit of infinite time of observation, there is no room for hysteresis in a finite size system at all. A quantitative analysis of spontaneous transitions and hysteresis in open systems is related to the nucleation phenomena [6] and is beyond the scope of this paper.

From figures 3–6, we conclude that CEDFT gives, in general, good agreement with the gauge cell and GCMC simulations for pores wider than about 3 nm. For smaller pores deviations become progressively more pronounced as expected. However, even for pores as small as 1–2 nm, the characteristic features of capillary condensation are still captured by CEDFT quite well. Note that the DFT adsorption isotherms feature the consecutive formation of adsorption layers associated with sigmoid swings indicating layering transitions. These transitions are common artefacts of the complete neglect of local density fluctuations in DFT. While these layering transitions make DFT isotherms visibly different from MC isotherms, the quantitative differences in integral parameters are negligible. Also, while the positions of spinodals in MC simulations and DFT practically coincide, DFT produces states of smaller density and larger compressibility in the vicinity of the liquid-like spinodal. This leads to exaggeration of the so-called superspinodal behaviour [63] associated with the existence of multiple states of equal average density which are seen in the DFT isotherm for the 5.54 nm pore.

6. Comparison of DFT and MC results with macroscopic capillary condensation theory

The classical scenario of capillary hysteresis [8, 13, 68, 69] in cylindrical geometry implies that the equilibrium capillary condensation and desorption are associated with the formation of a hemispherical meniscus in the channel while the spontaneous capillary condensation is associated with the formation of a cylindrical liquid film on the channel wall. The conditions of equilibrium and spontaneous condensation are given by the Kelvin–Cohan (KC) equations [68]:

$$RT \ln(P_e/P_0) = -\frac{2\gamma V_L}{R_P - h_e} \tag{6}$$

$$RT \ln(P_c/P_0) = -\frac{\gamma V_L}{R_P - h_c}. \tag{7}$$

Here P_e/P_0 and P_c/P_0 are the relative pressures of equilibrium condensation/desorption and spontaneous condensation, respectively; γ and V_L are the surface tension and the molar volume of the bulk liquid; R_P is the pore radius; and h_e and h_c are the adsorption film thicknesses at the relative pressures P_e/P_0 and P_c/P_0 respectively.

Let us return to figure 5. There are several features worth noticing. As the pore size increases, the line of liquid-like spinodal saturates at the value corresponding to the spinodal of the bulk liquid. DFT calculations performed for larger pores (up to 50 nm) show that

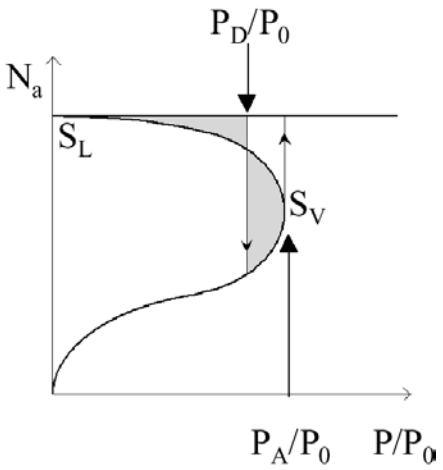

Figure 7. A schematic diagram of an adsorption isotherm according to the DBdB theory.

the line of equilibrium capillary condensation asymptotically approaches the KC equation (6) for the spherical meniscus and the line of spontaneous capillary condensation asymptotically approaches the KC equation (8) for the cylindrical meniscus; see below.

The deviations from the KC equations become appreciable for pores as large as 10 nm. The KC equations do not account for the interactions between the adsorption film and the substrate and thus does not consider the conditions of adsorption film stability which determine the onset of spontaneous capillary condensation. This shortcoming is overcome in the macroscopic theory of DBdB [7–9, 70].

According to Derjaguin [7, 70] the equilibrium thickness of the adsorbed film in a cylindrical pore is determined by the balance of the capillary and disjoining pressures and is given by

$$\Pi(h)V_{\mathrm{L}} + \frac{\gamma V_{\mathrm{L}}}{R_{\mathrm{P}} - h} = RT\ln(P_0/P). \tag{8}$$

The disjoining pressure $\Pi(h)$ caused by the fluid–solid interaction potential and the surface tension γ are assumed to be independent of the pore wall curvature. The disjoining pressure $\Pi(h)$ in equation (8) can be obtained from the adsorption isotherm on a flat surface. This approach is equivalent to the scheme used later by Broekhoff and de Boer [8, 9] to describe capillary condensation and is referred to as DBdB theory [35]. DBdB theory assumes also that the adsorption film and the condensed fluid are incompressible and have the density of the bulk liquid. It is equivalent to the Saam–Cole theory [69]. For many practical applications, the adsorption isotherm of a flat surface is approximated by the power law $\Pi(h) \propto h^{-m}$, known as the Frenkel–Halsey–Hill (FHH) equation [71].

For monotonic adsorption isotherms of FHH type, equation (8) implies a characteristic shape of adsorption isotherms for cylindrical pores, depicted in figure 7. The adsorption N_{a} as a function of the relative pressure P/P_0 has a van der Waals sigmoid shape. The ascending branch that corresponds to adsorption films turns over at the spinodal $\mathrm{S_V}$ determined from the condition of stability of films fulfilling equation (8). The limiting thickness $h = h_{\mathrm{cr}}$ of mechanically stable adsorption films is given by the algebraic equation

$$-\left(\frac{\mathrm{d}\Pi(h)}{\mathrm{d}h}\right)_{h=h_{\mathrm{cr}}} = \frac{\gamma}{(R_{\mathrm{P}} - h_{\mathrm{cr}})^2}. \tag{9}$$

In the DBdB method it is assumed that, as the vapour pressure increases, condensation occurs spontaneously when the limit of stability of the adsorbed films is achieved, i.e. at the spinodal S_V. Thus, the conditions of capillary condensation in an open-ended cylindrical pore are determined by the system of two equations (8) and (9).

The descending branch $S_V S_L$ corresponds to unstable cylindrical films with a progressively decreasing internal radius. This branch merges with the desorption branch as the vapour pressure vanishes. The desorption branch is represented by a plateau at the bulk liquid density due to the assumption of fluid incompressibility. The behaviour of the isotherm at low pressure is obviously unphysical; however, this region does not contribute appreciably to the results of thermodynamic integration for relatively wide pores.

Similarly to the classical KC scenario, desorption takes place at the equilibrium between the condensed fluid and the adsorption film. The condition of equilibrium is determined from the equality of grand thermodynamic potentials, or the Maxwell rule (5). Thus, desorption from an open-ended cylindrical capillary is determined by the condition of formation of the equilibrium meniscus given by the augmented Kelvin equation, known as the Derjaguin equation [7]:

$$RT \ln(P_0/P) = \frac{2\gamma V_L + \frac{2V_L}{(R_P - h_e)} \int_{h_e}^{R_P} (R_P - h)\Pi(h)\,\mathrm{d}h}{R_P - h_e}. \tag{10}$$

Here, h_e is the thickness of the adsorbed film in equilibrium with the meniscus, given by equation (8).

In our previous paper [35], we showed that the NLDFT adsorption isotherm of a flat surface can be approximated by the FHH equation in the region of polymolecular adsorption, and thus the effective disjoining pressure is given by

$$\Pi(h) = \frac{RT}{V_L}\frac{K}{h^m}. \tag{11}$$

For our case study, Ar on silica, $K = 73.17$ and $m = 2.665$, with h in Å and $V_L = 34.66$ cm^3 mol^{-1}, were chosen from the best fit of the NLDFT isotherm with the FHH equation [35].

Using equation (11) with the above parameters, we have determined the conditions of spontaneous capillary condensation from equations (8) and (9), and the conditions of desorption from equations (8) and (10). The results are presented in figure 8. The predictions of the DBdB theory smoothly merge with the NLDFT calculations for pores of 7–10 nm and larger. It is worth noting that the DBdB theory significantly extends the range of applicability of macroscopic theories compared with KC equations (1) and (2). However, the departure from the MC data for pores of 5 nm and smaller is quite appreciable. The macroscopic theory can be further improved by taking into account the fluid compressibility and dependences of the surface tension and the disjoining pressure on the pore wall curvature.

7. Correspondence of NLDFT results to experimental data

In a series of earlier publications [35–37], we demonstrated with various examples of capillary condensation of argon and nitrogen in open-ended cylindrical pores of mesoporous molecular sieves of MCM-41 [17, 18] and SBA-15 [72] types that the capillary condensation and desorption isotherms predicted by NLDFT agree remarkably well with experimental hysteretic data for pores wider than ∼5 nm. For pores smaller than ∼4 nm, experimental isotherms are reversible and the position of capillary condensation is predicted by the condition of equilibrium meniscus formation, equation (5). For intermediate pores, ∼4–5 nm, the experimental

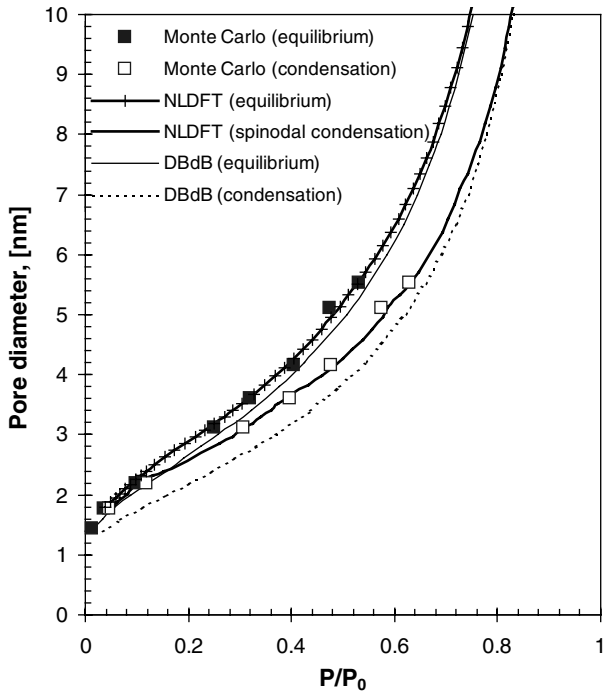

Figure 8. Bridging scales: capillary hysteresis of argon in cylindrical pores at 87.3 K. The pressures of condensation and desorption predicted by the NLDFT, gauge cell method, and DBdB theory.

hysteresis loop is narrower than that predicted by NLDFT, yet the experimental and theoretical desorption branches are quite close.

These conclusions are illustrated in figure 9, where we collected available experimental data on N_2 sorption on MCM-41 and SBA-15 types of material from different sources and compared with the NLDFT predictions of spontaneous and equilibrium capillary condensation transitions. The details of NLDFT calculations for this system were given in [11, 36, 37]. To show the prominent departures from conventional equations, the predictions of KC equations (6) and (7) are also given.

8. Conclusions

We show that the NLDFT efficiently spans the gap between the molecular simulations performed at the scale below ∼5 nm and the macroscopic thermodynamic equations. We applied NLDFT in the canonical ensemble to generate continuous adsorption isotherms which, at subcritical conditions, form sigmoid curves of van der Waals type. Tarazona's smooth density approximation was implemented to construct the free energy functional. The calculations were carried out for a series of cylindrical pores from 1 to 100 nm. The fluid–fluid and solid–fluid interaction parameters were chosen to represent argon and nitrogen sorption on silica. Capillary condensation of argon at its boiling temperature was selected as a case study due to the availability of MC data generated recently by the gauge cell MC method and also experimental data collected on reference mesoporous molecular sieves with uniform cylindrical pores.

The NLDFT isotherms agree remarkably well with the MC isotherms for pores wider than ∼3 nm. The condensed fluid density and the positions of equilibrium transitions and spinodals coincide within an experimentally negligible error. The density profiles are almost

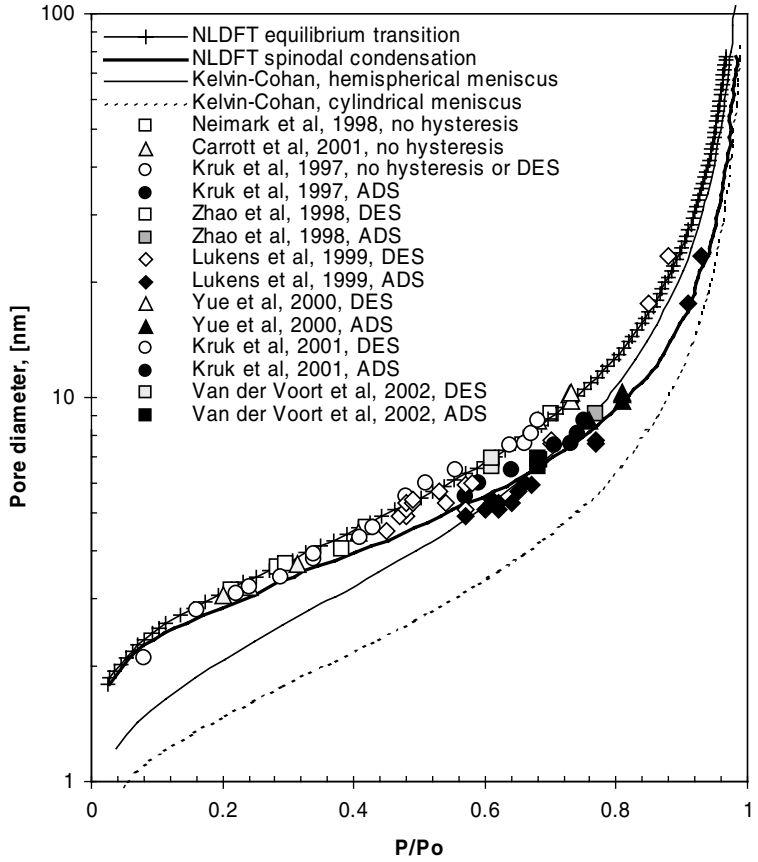

Figure 9. Relative pressures of the adsorption and desorption for N_2 at 77 K in open cylindrical pores in comparison with the experimental data [11, 73, 75–79] on ordered MCM-41 and SBA-15 nanoporous materials with cylindrical pores. Predictions of the macroscopic KC equation are also shown.

identical. Some deviations are found in the vicinity of the liquid-like spinodal; NLDFT liquid-like states are of lower density and larger compressibility. The overall behaviour of the isotherms in the regions of monolayer and multilayer formation is also quite good. However, the NLDFT isotherm exaggerates layering transitions producing artificial 'first-order' loops, whose contributions are luckily cancelled out during thermodynamic integration; thus they do not affect the overall course of the grand thermodynamic potential. Surprisingly, the two methods produce quantitatively similar labile states on the unstable backward branch of the isotherm. For sufficiently wide pores, canonical ensemble NLDFT revealed a peculiar behaviour: the existence of multiple states of equal density in the vicinity of the liquid-like spinodal. This observation was confirmed by MC simulations and is discussed in detail elsewhere [63]. For pores narrower than $\sim$3 nm, agreement between the theoretical and simulated isotherms progressively worsens; however, the major features, such as the positions of the equilibrium capillary condensation and spinodals, are captured satisfactorily even for pores as narrow as $\sim$2 nm.

The comparison of the results of GCMC simulations, which are performed without constraints on density fluctuations, with the CEDFT and gauge cell MC data provides a qualitative description of three experimentally observed regimes of capillary condensation:

supercritical, reversible, and hysteretic. Indeed, similarly to the experimental observations for GCMC simulations of Ar sorption at 87.4 K, the hysteresis critical pore size $D_{ch} \approx 2$ nm exceeds the critical pore size $D_{cc} \approx 1.5$ nm. While the critical pore size is determined by the temperature, pore geometry, and fluid–solid interactions, and does not depend on the experimental conditions, such as the observation time and the system size, the hysteresis critical pore size does depend on the scales of time and size which determine the level of admissible fluctuations and, consequently, the probability of nucleation. Thus, it is not surprising that since the level of fluctuations in experiments is drastically larger than in GCMC simulations, the experimental hysteresis critical pore size estimated as $\sim$4 nm significantly exceeds the hysteresis critical pore size obtained in simulations.

The MC and NLDFT results were compared with macroscopic theories of capillary condensation. Appreciable departures from the classical KC equations were found for pores as large as 10 nm. We checked the applicability of the DBdB theory, which employs the disjoining pressure to characterize the fluid–solid interactions. The isotherm of disjoining pressure for argon on silica was constructed from the adsorption isotherm on a flat surface calculated by means of NLDFT. The DBdB equations for the relations between the pressures of capillary condensation and desorption and the pore diameter agree fairly accurate with the NLDFT calculations for pores of 7–8 nm and larger.

We have also presented a comprehensive collection of experimental data on capillary condensation of nitrogen on mesoporous molecular sieves of MCM-41 and SBA-15 types, which contain uniform cylindrical pores, and demonstrated good agreement of NLDFT predictions with experimental data.

That is, we draw a final conclusion that NLDFT with properly chosen parameters for intermolecular interactions correctly approximates results of MC simulations (shift of vapour–liquid equilibrium, spinodals, density profiles, adsorption isotherms) for pores wider than about 2 nm. On the other hand, NLDFT smoothly merges (above 7–10 nm) with the DBdB equations of capillary condensation and desorption, thus bridging scales from molecular simulations to macroscopic description.

Acknowledgments

This work was supported in parts by the TRI/Princeton exploratory research program, EPA (grant R825959-010), and Quantachrome Corporation.

References

[1] Evans R 1992 *Fundamentals of Inhomogeneous Fluids* ed D Henderson (New York: Dekker) ch 5
[2] Tarazona P, Marconi U M B and Evans R 1987 *Mol. Phys.* **60** 573–95
[3] Tarazona P 1985 *Phys. Rev.* A **31** 2672–9
[4] Ravikovitch P I, O'Domhnail S C, Neimark A V, Schuth F and Unger K K 1995 *Langmuir* **11** 4765–72
[5] Ravikovitch P I, Vishnyakov A and Neimark A V 2001 *Phys. Rev.* E **6401** 011602
[6] Vishnyakov A and Neimark A V 2001 *J. Phys. Chem.* B **105** 7009–20
[7] Derjaguin B V 1940 *Acta Phys.-Chim.* **12** 181–200
[8] Broekhoff J and de Boer J H 1967 *J. Catal.* **9** 8–28
[9] Broekhoff J and de Boer J H 1968 *J. Catal.* **10** 368–480
[10] Neimark A V and Vishnyakov A 2000 *Phys. Rev.* E **62** 4611–22
[11] Neimark A V, Ravikovitch P I, Grun M, Schuth F and Unger K K 1998 *J. Colloid Interface Sci.* **207** 159–69
[12] Kruk M and Jaroniec M 2000 *Chem. Mater.* **12** 222–30
[13] Everett D H 1967 *The Solid–Gas Interface* vol 2, ed E A Flood (New York: Dekker) ch 36
[14] Gelb L D, Gubbins K E, Radhakrishnan R and Sliwinska-Bartkowiak M 1999 *Rep. Prog. Phys.* **62** 1573–659
[15] Evans R, Marconi U M B and Tarazona P 1986 *J. Chem. Soc. Faraday Trans.* **82** 1763–87
[16] Ball P C and Evans R 1989 *Langmuir* **5** 714–23

[17] Kresge C T, Leonowicz M E, Roth W J, Vartuli J C and Beck J S 1992 *Nature* **359** 710–12
[18] Beck J S, Vartuli J C, Roth W J, Leonowicz M E, Kresge C T, Schmitt K D, Chu C T W, Olson D H, Sheppard E W, McCullen S B, Higgins J B and Schlenker J L 1992 *J. Am. Chem. Soc.* **114** 10834–43
[19] Morishige K and Shikimi M 1998 *J. Chem. Phys.* **108** 7821–4
[20] Morishige K and Masataka I 2002 *J. Chem. Phys.* **117** 8036–41
[21] Landau L D and Lifshitz E M 1959 *Statistical Physics* vol 1 (Oxford: Pergamon)
[22] Gelb L D 2002 *Mol. Phys.* **100** 2049–57
[23] Liu A J and Grest G S 1991 *Phys. Rev.* A **44** R7894–7
[24] Liu A J, Durian D J, Herbolzheimer E and Safran S A 1990 *Phys. Rev. Lett.* **65** 1897–900
[25] Lin M Y, Sinha S K, Drake J M, Wu X I, Thiyagarajan P and Stanley H B 1994 *Phys. Rev. Lett.* **72** 2207–10
[26] Gelb L D and Gubbins K E 1997 *Phys. Rev.* E **56** 3185–96
[27] Gelb L D and Gubbins K E 1997 *Abstracts of Papers of the American Chemical Society* **213** 349-PHYS
[28] Gelb L D and Gubbins K E 1997 *Phys. Rev.* E **55** R1290–3
[29] Penrose O and Lebowitz J L 1971 *J. Stat. Phys.* **3** 211
[30] Penrose O and Lebowitz J L 1987 Towards a rigorous molecular theory of metastability *Fluctuation Phenomena* ed J L Lebowitz and E Montroll (Amsterdam: North-Holland)
[31] Corti D S and Debenedetti P G 1994 *Chem. Eng. Sci.* **49** 2717–34
[32] Stillinger F H 1995 *Phys. Rev.* E **52** 4685
[33] Corti D S, Debenedetti P G, Sastry S and Stillinger F H 1997 *Phys. Rev.* E **55** 5522
[34] Ravikovitch P I, Wei D, Chueh W T, Haller G L and Neimark A V 1997 *J. Phys. Chem.* B **101** 3671–9
[35] Neimark A V and Ravikovitch P I 2001 *Microporous Mesoporous Mater.* **44** 697–707
[36] Ravikovitch P I and Neimark A V 2001 *Colloids Surf.* A **187** 11–21
[37] Ravikovitch P I and Neimark A V 2001 *J. Phys. Chem.* B **105** 6817–23
[38] Ravikovitch P I and Neimark A V 2002 *Langmuir* **18** 1550–60
[39] Rosenfeld Y 1989 *Phys. Rev. Lett.* **63** 980–3
[40] Kierlik E and Rosinberg M L 1990 *Phys. Rev.* A **42** 3382–7
[41] Curtin W A and Ashcroft N W 1985 *Phys. Rev.* A **32** 2909–19
[42] Rosenfeld Y, Schmidt M, Lowen H and Tarazona P 1997 *Phys. Rev.* E **55** 4245–63
[43] Evans R 1979 *Adv. Phys.* **28** 143–200
[44] Davis H T 1996 *Statistical Mechanics of Phases, Interfaces, and Thin Films* (New York: Wiley)
[45] Evans R 1990 *J. Phys.: Condens. Matter* **2** 8989–9007
[46] Lastoskie C, Gubbins K E and Quirke N 1993 *J. Phys. Chem.* **97** 4786–96
[47] Olivier J P 1995 *J. Porous Mater.* **2** 217
[48] Ravikovitch P I, Haller G L and Neimark A V 1998 *Adv. Colloid Interface Sci.* **77** 203–26
[49] Neimark A V and Ravikovitch P I 1997 *Langmuir* **13** 5148–60
[50] Vishnyakov A, Ravikovitch P I and Neimark A V 1999 *Langmuir* **15** 8736–42
[51] Ravikovitch P I, Vishnyakov A, Russo R and Neimark A V 2000 *Langmuir* **16** 2311–20
[52] Talanquer V and Oxtoby D W 1995 *J. Phys. Chem.* **99** 2865–74
[53] Neimark A V and Ravikovitch P I 1998 Density functional theory for studies of multiple states of inhomogeneous fluids at solid surfaces and in pores *Microscopic Simulation of Interfacial Phenomena in Solids and Liquids* vol 492, ed S R Phillpot, P D Bristowe, D G Stroud and J R Smith (Warrendale, PA: Materials Research Society) pp 27–33
[54] Gonzalez A, White J A, Roman F L, Velasco S and Evans R 1997 *Phys. Rev. Lett.* **79** 2466–9
[55] Aranovich G L and Donohue M D 1999 *Phys. Rev.* E **60** 5552–60
[56] Malanoski A P and Swol F V 2000 Paper 157a *The AIChE 2000 Annual Mtg (Los Angeles, CA)*
[57] Frink L J D and Salinger A G 2002 *J. Phys.: Condens. Matter* **14** 2167–87
[58] Hernando J A and Blum L 2001 *J. Phys.: Condens. Matter* **13** L577–82
[59] Maier R W and Stadtherr M A 2001 *AICHE J.* **47** 1874–84
[60] Gonzalez A, White J A and Roman F L 1998 *J. Chem. Phys.* **109** 3637–50
[61] White J A, Gonzalez A, Roman F L and Velasco S 2000 *Phys. Rev. Lett.* **84** 1220–3
[62] Hernando J A 2002 *J. Phys.: Condens. Matter* **14** 303–17
[63] Neimark A V, Ravikovitch P I and Vishnyakov A 2002 *Phys. Rev.* E **65** 031505
[64] Hohenberg P and Kohn W 1964 *Phys. Rev.* B **136** B864
[65] Kohn W, Becke A D and Parr R G 1996 *J. Phys. Chem.* **100** 12974–80
[66] Lebowitz J L and Percus J K 1961 *Phys. Rev.* **122** 1675
[67] Press W H, Teukolsky S A, Vetterling W T and Flannery B P 1992 *Numerical Recipes in C. The Art of Scientific Computing* 2nd edn (Cambridge: Cambridge University Press)
[68] Cohan L J 1938 *J. Am. Chem. Soc.* **60** 433

[69] Saam W F and Cole M W 1975 *Phys. Rev.* B **11** 1086–105
[70] Derjaguin B V and Churaev N V 1976 *J. Colloid Interface Sci.* **54** 157
[71] Gregg S J and Sing K S W 1982 *Adsorption, Surface Area and Porosity* (New York: Academic)
[72] Zhao D Y, Feng J L, Huo Q S, Melosh N, Fredrickson G H, Chmelka B F and Stucky G D 1998 *Science* **279** 548–52
[73] Kruk M, Jaroniec M and Sayari A 1997 *J. Phys. Chem.* B **101** 583–9
[74] Peterson B K and Gubbins K E 1987 *Mol. Phys.* **62** 215–26
[75] Lukens W W, Schmidt-Winkel P, Zhao D Y, Feng J L and Stucky G D 1999 *Langmuir* **15** 5403–9
[76] Yue Y H, Gedeon A, Bonardet J L, D'Espinose J B, Melosh N and Fraissard J 2000 *Stud. Surf. Sci. Catal.* **129** 209–18
[77] Sayari A, Liu P, Kruk M and Jaroniec M 1997 *Chem. Mater.* **9** 2499–506
[78] Carrott M, Candeias A J E, Carrott P J M, Ravikovitch P I, Neimark A V and Sequeira A D 2001 *Microporous Mesoporous Mater.* **47** 323–37
[79] Van Der Voort P, Ravikovitch P I, De Jong K P, Benjelloun M, Van Bavel E, Janssen A H, Neimark A V, Weckhuysen B M and Vansant E F 2002 *J. Phys. Chem.* B **106** 5873–7